Published in final edited form as:
Magn Reson Med. 2011 February ; 65(2): 377–384. doi:10.1002/mrm.22673.

Mapping proteoglycan-bound water in cartilage: improved specificity of matrix assessment using multiexponential transverse relaxation analysis

David A. Reiter[1], **Remigio A. Roque**[1], **Ping-Chang Lin**[1], **Onyi Irrechukwu**[1], **Stephen Doty**[2], **Dan Longo**[3], **Nancy Pleshko**[4], and **Richard G. Spencer**[1]

[1]Magnetic Resonance Imaging and Spectroscopy Section, National Institute on Aging, National Institutes of Health, Baltimore, MD 21224

[2]Research Division, Microscopy Core Facility, Hospital for Special Surgery, New York, NY 10021

[3]Office of the Scientific Director, National Institute on Aging, National Institutes of Health, Baltimore, MD 21224

[4]Department of Mechanical Engineering, Temple University, Philadelphia, PA 19122

Abstract

Association of MR parameters with cartilage matrix components remains an area of ongoing investigation. Multiexponential analysis of non-localized transverse relaxation data has previously been used to quantify water compartments associated with matrix macromolecules in cartilage. We extend this to mapping the proteoglycan-bound water fraction (w_{PG}) in cartilage, using mature and young bovine nasal cartilage model systems, towards the goal of matrix component-specific imaging. w_{PG} from mature and young bovine nasal cartilage was 0.3±0.04 and 0.22±0.06, respectively, in agreement with biochemically-derived proteoglycan content and proteoglycan-to-water weight ratios. Fourier transform infrared imaging spectroscopic-derived proteoglycan maps normalized by water content (IR-PG_{ww}) showed spatial correspondence with w_{PG} maps. Extensive simulation analysis demonstrated that the accuracy and precision of our determination of w_{PG} was within 2%, which is substantially smaller than the observed tissue differences. Our results demonstrate the feasibility of performing imaging-based multiexponential analysis of transverse relaxation data to map proteoglycan in cartilage.

Keywords

transverse relaxation; proteoglycan mapping; multiexponential relaxation; cartilage

Introduction

Nondestructive analysis of cartilage through association of MR outcome measures with cartilage degradation remains an area of active investigation. T_1, T_2, magnetization exchange rate and ratio, apparent diffusion coefficient, and $T_{1\rho}$ all show sensitivity to changes in matrix composition (1–3), but lack specificity to particular matrix components (4–7).

Address correspondence to: Richard G. Spencer, Magnetic Resonance Imaging and Spectroscopy Section, GRC 4D-06, National Institute on Aging, National Institutes on Health, Baltimore, MD 21224, spencer@helix.nih.gov, 410-558-8226, FAX: 410-558-8318.

Multiexponential relaxation analysis has been used to detect and quantify water compartmentation in biological tissues associated with tissue microstructure, providing information on macromolecular content (8–10). As compared to localized measurements, non-localized MR experiments permit more sensitive characterization of multiple relaxation components and detection of more rapidly relaxing components (9–11) due primarily to greater SNR, shorter pulse lengths, and shorter echo times. However, results from non-localized measurements are difficult to interpret in anisotropic and heterogeneous tissues such as articular cartilage, as relaxation components can reflect either regional tissue differences or water compartments related to different microscopic environments.

In previous work, we applied multiexponential analysis to non-localized T_2 relaxation data to identify water fractions reflecting macromolecular composition (12,13). Bovine nasal cartilage (BNC) was an appropriate tissue model in that study, since it has a matrix composition similar to articular cartilage but is largely isotropic and homogeneous, permitting interpretation of the non-localized measurements in terms of tissue microstructure. Two of the T_2 components identified were assigned to water tightly bound to proteoglycan (C_{PG}) and bulk water loosely bound to matrix macromolecules (C_{LB}) and had T_2s of ~25 ms and ~96 ms, respectively (12). We showed that even with the relatively long TEs (~10ms) required for imaging, these components could be reliably detected with reasonable values of SNR. These results indicated the potential extension of multiexponential analysis of T_2 relaxation data to quantify regional proteoglycan (PG) distribution in cartilage.

Accordingly, in the present work, we apply multiexponential T_2 analysis to map the PG-bound water compartment in cartilage towards the goal of MR-based matrix component-specific imaging. We demonstrate this approach on BNC taken from animals of different ages and therefore exhibiting different macromolecular composition. MR results are supported with biochemical analysis to quantify the bulk amounts of water, PG, and collagen per sample. In addition, Fourier transform infrared imaging spectroscopy (FT-IRIS) was used to provide spatially resolved quantitative maps of PG and collagen content for comparison with MR results. We also performed extensive multiexponential analysis of simulated relaxation data to determine the accuracy in quantifying component T_2s and fractions given the available SNR and acquisition parameters required for imaging (12,14–16). Finally, we note that nondestructive matrix assessment is primarily of interest in articular cartilage. Therefore, we also apply multiexponential T_2 analysis to young bovine patellar cartilage, showing that this approach can readily be applied to articular cartilage.

Methods

Sample Harvest and Preparation

BNC plugs—BNC plugs (diameter = 6 mm) were excised from the nasal septum of a young (approx. 3 months old) and a skeletally mature (approx. 2 years old) cow (Green Village Packing, Green Village, NJ), were moistened with Dulbecco's Phosphate Buffered Saline (DPBS) and stored at 4°C until imaged. Prior to imaging, each plug was removed individually and excess surface water was removed by gently blotting the sample. All samples were tested within 5 days of harvest.

Bovine patella—A patella was excised from the stifle joint of a young cow (approx. 3 months old; Green Village Packing) and kept moist in DPBS at 4°C until experimentation. Again, excess surface water was removed prior to imaging.

MRI

Data were acquired with a 9.4T Bruker DMX NMR spectrometer (Bruker Biospin, GmbH, Rheinstetten, Germany) at 4°C. All samples were immersed in Fluorinert FC-77 (Sigma-Aldrich, St. Louis, MO) to maintain sample hydration while imaging.

BNC plugs—A custom Ultem sample holder was used to position the centers of 3 BNC plugs along the diameter of a 25 mm NMR tube permitting acquisition of a single mid-sagittal slice through all samples at the instrument iso-center. Relaxation data were acquired using a single slice multi-echo CPMG imaging sequence with the following acquisition parameters: TE/TR = 5.5ms/5s, 128 echoes, slice thickness = 2mm, FOV = 3×3 cm, matrix = 128×128, NEX = 32. The even echoes were analyzed resulting in an effective TE = 11 ms and 64 echoes.

Patella—Relaxation data were measured using the same resonator, sequence and acquisition parameters as in BNC but with a 3mm slice thickness.

Fitting of T_2 Relaxation Data

The regularized non-negative least squares (NNLS) method was used for multiexponential T_2 analysis as previously described (12). The NNLS method makes no *a priori* assumptions about the number of relaxation components present. Conventional monoexponential analysis was also performed. All fits were performed on an individual pixel basis producing monoexponential T_2 and multiexponential T_2 distributions at each pixel. Multiexponential T_2 and magnetization fraction maps were generated using the first moment and the integrated area for each identified component of the T_2 distribution. PG-bound water maps were calculated as a ratio $w_{PG} = \rho_{PG}/(\rho_{LB} + \rho_{PG})$, where ρ represents component fraction. Average T_2s and fractions derived from averaging pixel values over each sample were used to compare young and mature tissue. Fits and other analyses were implemented in MATLAB (MathWorks, Natick, MA).

Simulation of T_2 Relaxation Data

Analysis of simulated data was performed to ensure the admissibility of our results, as described previously (12). Reliability was defined as correctly identifying the simulated number of T_2 components, accuracy was defined by percent error of the derived T_2s and weights, and precision was defined as their coefficient of variation (CV). Data were simulated using TE = 11 ms, 64 echoes, and average experimental values for SNR and the component T_2's and weights (see below). The reliability, accuracy, and precision of the results were evaluated over 100 trials with different noise realizations for each SNR value.

Biochemical Analysis

Sulfated glycosaminoglycans (sGAG) and hydroxyproline (HP) content were assessed using standard assays. After imaging, BNC samples were cut in half along the imaging plane permitting biochemical and FT-IRIS analysis on adjacent halves of each sample. The sections reserved for biochemical analysis were digested in 100mM ammonium acetate buffer. sGAG content was quantified using the 1,9-dimethylmethylene blue assay (17). Total collagen content was quantified using the colorimetric chloramine-T/p-dimethylaminobenzaldehyde assay and a HP standard (18).

Fourier Transform Infrared Imaging Spectroscopy (FT-IRIS)

BNC sample halves reserved for FT-IRIS were stored in 70% isopropyl alcohol and 1% cetylpyridinium chloride (Sigma-Aldrich, St. Louis, MO) and embedded in paraffin. Six micron thick sections were taken from the surface corresponding to the MR imaging plane

and examined using a Spectrum SpotLight FT-IR imaging system (Perkin-Elmer, Bucks, UK) (19). A mid-IR spectrum from 800 to 4000 cm^{-1} with 8 cm^{-1} spectral resolution was obtained from each 25 × 25 μm imaging pixel.

The amide I band and proteoglycan sugar band areas were calculated by integrating in the ranges of 1592 – 1744 cm^{-1} and 960 – 1184 cm^{-1}, respectively, after baseline subtraction (19,20). These areas were used to generate maps of collagen and proteoglycan content, respectively (ISys software v3.1, Spectral Dimensions Olney, MD). Average intensity values over the sample were used for quantifying total PG and collagen content within each sample.

FT-IRIS images provide maps of specific resonances within matrix molecules, essentially independent of water content. In contrast, MR-derived w_{PG} maps are proportional to total water content. To allow comparison of these two modalities, we normalized IR-derived PG maps for a given sample by its biochemically derived water content. This normalization was calculated as the sum of the biochemically-derived water weight divided by the total sample wet weight.

Statistical Analysis

Data for young and mature BNC are reported as mean ± standard deviation (SD) with statistical significance taken as $p < 0.05$ according to unpaired t-test comparisons.

Results

Table 1 shows the accuracy and precision of component T_2s and fraction weights (w) determined from simulations, using the average SNR from young and mature BNC. The input simulation values for component T_2s and weights corresponded to experimentally derived values for the two T_2 components found in both young and mature BNC. The more rapidly-relaxing component was assigned to PG-bound water (C_{PG}) while the slowly relaxing component was assigned to bulk water loosely associated with matrix macromolecules (C_{LB}) (13). Reliability for both young and mature groups was 100%, indicating the robustness in resolving the two components under the simulated conditions. Component fraction w_{PG} showed the largest error, although the accuracy in both young and mature groups was within ~2%. The precision of both $T_{2,PG}$ and w_{PG} showed errors of ~1.5% for both the young and mature groups. All other errors were <1%. These simulations indicate excellent reliability, accuracy, and precision for resolving PG-bound water and bulk water T_2s and component fractions using our acquisition parameters.

Biochemical analysis (Table 2) showed significantly greater water content in young samples compared to mature samples, with water fractions 77.9 ± 0.8% and 65.7 ± 2.7%, respectively. Young samples also had a significantly greater sGAG per dry weight, while sGAG per wet weight was not different ($p=0.37$) between mature and young BNC (123 ± 19.4 ug/mg and 111 ± 9.2 ug/mg, respectively); this is primarily due to lower water content in mature samples. Mature BNC showed a trend ($p = 0.09$) towards greater HP per dry weight compared to young BNC (52.2 ± 9.9 ug/mg and 42.4 ± 3.2 ug/mg, respectively). These differences are consistent with the matrix changes known to occur in cartilage development.

FT-IRIS and MRI results are shown in Table 3. FT-IRIS showed no significant differences ($p=0.36$) in PG content between young (2953 ± 100) and mature (2889 ± 78) BNC. The FT-IRIS-derived collagen content in mature samples was significantly greater than in young BNC, with values 3180 ± 79 and 2688 ± 37, respectively. These FT-IRIS-derived matrix results are consistent with the biochemically-derived matrix content per dry weight; as

discussed, dry weight comparisons are the most appropriate for comparison to dehydrated FT-IRIS sections. The normalized FT-IRIS-derived PG content (IR-PG_{ww}) was significantly greater in mature BNC compared to young BNC with integrated resonance areas of 4397 ± 123 and 3801 ± 137, respectively; these values are most appropriately compared with biochemically derived sGAG per wet weight and show a good correspondence.

Conventional monoexponential T_2 in young BNC was significantly greater than in mature BNC, with T_2s of 84.5 ± 10.5 ms and 64.8 ± 6.1 ms, respectively, consistent with differences in water content. Multiexponential analysis consistently demonstrated two components: a more rapidly relaxing component assigned to PG-bound water, $T_{2,PG}$, and a more slowly relaxing component assigned to bulk water that is more loosely bound to matrix macromolecules, $T_{2,LB}$. The magnetization fraction w_{PG} in mature BNC was significantly greater compared to young BNC (0.31 ± 0.04 and 0.22 ± 0.06, respectively). This relationship is consistent with the biochemically derived sGAG and IR-PG_{ww}, indicating consistency across all modalities.

As discussed above, IR-PG_{ww} images represent a direct map of tissue PG normalized by wet weight. These maps are expected to correspond to our MR-derived w_{PG} maps. This correspondence is shown in Figure 1 in which both modalities reflect less proteoglycan in the young sample compared to the mature sample. In addition, an approximate spatial correspondence is readily seen between the two modalities; in both young and mature samples, regions of greater IR-PG_{ww} also show greater w_{PG}. Limitations on this spatial correspondence include the large differences in slice thickness between the MR and IR studies.

The specificity of the w_{PG} measurement for PG is shown in Figure 2. Whole sample averages of w_{pg} are plotted against IR-PG_{ww}, indicating a significant correlation ($r = 0.72$, $p = 0.046$) between these two measurements.

$T_{2,mono}$ maps of articular cartilage are often presented as indirect indicators of macromolecular density. Multiexponential T_2 analysis permits the more direct mapping of w_{PG}, a water fraction corresponding specifically to PG distribution.

Figure 3 shows mono- and multiexponential T_2 maps obtained from a sagittal view of the bovine patella with the articular surface at the top. Monoexponential T_2 shows the expected non-specific decease with depth. PG-specific $T_{2,PG}$ and are water fraction, w_{PG}, maps are shown in Figs 3b and 3c, while $T_{2,LB}$ and w_{LB} shown in Figs. 3d and 3e. $T_{2,LB}$ shows a pronounced decrease with depth, consistent with the known decrease in water content with depth as is also seen more directly in Fig. 3e. In contrast, w_{PG} increases with depth, consistent with its known distribution within articular cartilage.

Discussion

Using non-localized experiments, we have previously demonstrated the improved specificity of multiexponential as compared to monoexponential T_2 analysis under a wide variety of enzymatic conditions. In particular, the multiexponential approach demonstrated changes in macromolecule-associated water compartmentation consistent with the known actions of a several enzymatic degradation protocols, while monoexponential T_2 analysis showed only a non-specific increase in T_2 (13).

The non-localized CPMG measurements used in this previous work enabled the use of shorter echo times, resulting in detection of T_2s ranging from 1ms to several hundred milliseconds. However, the PG-associated components exhibit T_2s detectable using the longer TEs required by our imaging sequence (~10ms). In particular, the two components

we have assigned to PG-bound water (C_{PG}) and water loosely associated with matrix macromolecules (C_{LB}) exhibited T_2s of ~25 ms and ~96 ms, respectively (13), supporting our ability to map C_{PG} and C_{LB} in the current work. Further support was provided by biochemical analysis for PG content, as well as through comparison with bulk and spatially resolved FT-IRIS measurements of matrix components. Finally, maps of $T_{2,LB}$, w_{LB}, $T_{2,PG}$ and w_{PG}, maps were derived which were consistent with known gradations of PG and water content.

It is well-established that several factors influence the ability to accurately detect and quantify T_2 components using NNLS, including SNR, acquisition parameters, and tissue component T_2 and fractions (12,14–16). Therefore, simulations are critical for determining the accuracy of the results derived in a particular experimental protocol. Our simulations indicate excellent accuracy and precision under the experimental conditions and tissue characteristics present in this study. For example, the accuracy and precision for quantifying w_{PG} was within ~2%, which was much smaller than the ~41% difference in this parameter seen between mature and young BNC.

Assessment of BNC from young and mature animals tested the ability of the multiexponential analysis to detect subtle differences in macromolecular content. Young samples had greater water content and sGAG per dry weight while mature samples had greater HP by dry weight and sGAG per wet weight, consistent with age related differences previously reported (21,22). Furthermore, as reflected by our biochemically- and FT-IRIS-derived sGAG results, BNC has comparable macromolecular composition to articular cartilage (21) but lacks the high degree of heterogeneity and anisotropy of articular cartilage, reducing the influence of such confounding factors in multiexponential T_2 component analysis (23).

The MR-derived w_{PG} content was consistent with biochemically-derived PG content, showing greater PG content per wet weight in mature BNC. In a previous NMR study of proteoglycan hydration in articular cartilage, Ghiassi-Nejad et al. report the weight ratios of 1.1 for PG-bound water to PG, and 3.6 for the weight ratio of loosely associated water to PG (24). Their results reflect a ~0.23 fraction of PG-bound water to total water, comparable to our w_{PG} results in Table 3. Using the biochemical composition of BNC from Table 2 and assuming the same weight ratios as Ghiassi-Nejad et al., fractions of PG-bound water to total water for young and mature BNC are ~0.20 and ~0.33, respectively; these values closely correspond to the MR-derived fractions in Table 3 of 0.22 and 0.31, respectively. This quantitative correspondence between biochemistry and MR-derived PG content indicate the potential for multiexponential T_2 analysis to assay cartilage PG content.

FT-IRIS provides a particularly suitable validation for MR-derived proteoglycan mapping due to its ability to create semi-quantitative matrix component-specific maps (20). Indeed, FT-IRIS results of proteoglycan and collagen content in young and mature BNC are consistent with the biochemically-derived content per dry weight. Because mid-IR FT-IRIS, as used in this study, measures specific molecular resonances of dry matrix compounds largely independent of water content, PG measurements were normalized by sample water content for comparison to MR-derived proteoglycan content.

Spatial correspondence between MR-derived and FT-IRIS-derived PG content was visualized by selecting FT-IRIS sections which closely corresponded to MR image slices. Figure 1 shows representative FT-IRIS- and MR-derived PG maps from a young and mature BNC sample. Both modalities indicate greater PG per wet weight in the mature sample (Fig 1, Table 3). These modalities show good spatial agreement in the distribution of PG within each sample, although the correspondence between these two modalities is limited for

several reasons. First, although water is non-uniformly distributed throughout the sample, our normalization of the FT-IRIS-derived PG maps used whole-sample biochemical data. Subsequent studies can address this through use of localized water normalization based, for example, on MR proton density maps. Second, the MR slices were 2 mm in thickness, while the sections used for FT-IRIS were only 6 μm thick. Similar discrepancies attributed to partial volume effects have been reported when comparing histological sections stained for myelin content with MR-derived myelin water maps (25); although there was good qualitative correspondence, small lesions could be visualized with histology, while the MR maps showed a less definitive absence of myelin water. Reduction of MR slice thickness, perhaps through use of 3D imaging sequences, would be expected to improve the correspondence between MR and FT-IRIS derived maps. Although the difference in slice thickness is unavoidable, the MR technique by itself will be evidently be able to produce a map reflecting mean PG through a section on the order of, or less than, 0.5 mm thickness under typical conditions.

Linear regression was used to quantitatively evaluate the relationship between IR-PG_{ww} and w_{PG}, image intensities averaged over each sample (Fig. 2), and indicated a good correlation. Again, partial volume effects are expected to reduce this correlation. Indeed, comparable correlations between the optical density of histological sections stained for myelin content and MR-derived myelin water content have been reported, with limitations on the correlation attributed to partial volume effects (26).

Although the extensive analysis of BNC we have presented demonstrates a good correspondence between MR-derived PG-bound water fraction and biochemically- and FT-IRIS-derived PG content, the primary interest in this technique will be in studies of articular cartilage. Therefore, evaluation of bovine patellar cartilage was also performed. The conventional monoexponential T_2 map (Fig. 3a) shows a depth-dependence which could be attributed to several intrinsic tissue properties known to vary with depth such as collagen fiber orientation, hydration, and macromolecular content. In contrast, multiexponential T_2 analysis provides specific maps of w_{PG} and w_{LB} which reflect the known variation of PG and water content with depth (6,27). In terms of quantification, the bovine patellar w_{PG} fractions also reflect slightly lower PG content in comparison to BNC, consistent with biochemically-determined differences between BNC and articular cartilage (23).

In conclusion, the multiexponential approach described herein permits the mapping of matrix component-specific water fractions in cartilage using a standard MRI acquisition sequence. w_{PG} maps produced in this way were sensitive to age-related variations in PG content. Results were validated both by simulations and by other experimental modalities. Thus, multiexponential T_2 analysis provides a new method for mapping cartilage matrix composition that does not require use of specialized MR pulse sequences and hardware, or exogenous contrast agents (28–30).

Acknowledgments

This work was supported by the Intramural Research Program of the NIH, National Institute on Aging, and by NIH R01 EB000744 (NP). We acknowledge Mila Spevak and Orla O'Shea of the Hospital for Special Surgery for assistance with the collection of histologic and FT-IRIS data through the HSS Musculoskeletal Repair and Regeneration Core Facility NIH AR046121.

References

1. Burstein D, Bashir A, Gray ML. MRI techniques in early stages of cartilage disease. Investigative Radiology. 2000; 35(10):622–638. [PubMed: 11041156]

2. Laurent D, Wasvary J, Yin JY, Rudin M, Pellas TC, O'Byrne E. Quantitative and qualitative assessment of articular cartilage in the goat knee with magnetization transfer imaging. Magnetic Resonance Imaging. 2001; 19(10):1279–1286. [PubMed: 11804755]
3. Mlynarik V, Sulzbacher I, Bittsansky M, Fuiko R, Trattnig S. Investigation of apparent diffusion constant as an indicator of early degenerative disease in articular cartilage. Journal of Magnetic Resonance Imaging. 2003; 17(4):440–444. [PubMed: 12655583]
4. Lin PC, Reiter DA, Spencer RG. Sensitivity and specificity of univariate MRI analysis of experimentally degraded cartilage. Magnetic Resonance in Medicine. 2009
5. Menezes NM, Gray ML, Hartke JR, Burstein D. T2 and T1rho MRI in articular cartilage systems. Magnetic Resonance in Medicine. 2004; 51(3):503–509. [PubMed: 15004791]
6. Nissi MJ, Toyras J, Laasanen MS, Rieppo J, Saarakkala S, Lappalainen R, Jurvelin JS, Nieminen MT. Proteoglycan and collagen sensitive MRI evaluation of normal and degenerated articular cartilage. Journal of Orthopaedic Research. 2004; 22(3):557–564. [PubMed: 15099635]
7. Lin PC, Reiter DA, Spencer RG. Classification of degraded cartilage through multiparametric MRI analysis. Journal Of Magnetic Resonance. 2009; 201(1):61–71. [PubMed: 19762258]
8. Ababneh Z, Beloeil H, Berde CB, Gambarota G, Maier SE, Mulkern RV. Biexponential parameterization of diffusion and T2 relaxation decay curves in a rat muscle edema model: Decay curve components and water compartments. Magnetic Resonance in Medicine. 2005; 54(3):524–531. [PubMed: 16086363]
9. Graham SJ, Ness S, Hamilton BS, Bronskill MJ. Magnetic resonance properties of ex vivo breast tissue at 1.5 T. Magnetic Resonance in Medicine. 1997; 38(4):669–677. [PubMed: 9324335]
10. Nightingale T, MacKay A, Pearce RH, Whittall KP, Flak B. A model of unloaded human intervertebral disk based on NMR relaxation. Magnetic Resonance in Medicine. 2000; 43(1):34–44. [PubMed: 10642729]
11. English AE, Joy MLG, Henkelman RM. Pulsed NMR relaxometry of striated-muscle fibers. Magnetic Resonance in Medicine. 1991; 21(2):264–281. [PubMed: 1745125]
12. Reiter DA, Lin PC, Fishbein KW, Spencer RG. Multicomponent T2 relaxation analysis in cartilage. Magnetic Resonance in Medicine. 2009; 61(4):803–809. [PubMed: 19189393]
13. Reiter, DA.; Roque, RA.; Lin, PC.; Irrechukwu, O.; Pleshko, N.; Spencer, RG. Improved specificity of cartilage matrix assessment using multiexponential T2 parameter maps with validation by Fourier-transform infrared spectroscopic imaging. 17th annual meeting of the ISMRM; Honolulu, Hawai. 2009. p. 72
14. Anastasiou A, Hall LD. Optimisation of T2 and M0 measurements of bi-exponential systems. Magnetic Resonance Imaging. 2004; 22(1):67–80. [PubMed: 14972396]
15. Dula AN, Gochberg DF, Does MD. Optimal echo spacing for multi-echo imaging measurements of Bi-exponential T2 relaxation. Journal of Magnetic Resonance. 2009; 196(2):149–156. [PubMed: 19028432]
16. Graham SJ, Stanchev PL, Bronskill MJ. Criteria for analysis of multicomponent tissue T2 relaxation data. Magnetic Resonance in Medicine. 1996; 35(3):370–378. [PubMed: 8699949]
17. Farndale RW, Buttle DJ, Barrett AJ. Improved quantitation and discrimination of sulfated glycosaminoglycans by use of dimethylmethylene Blue. Biochimica et Biophysica Acta. 1986; 883(2):173–177. [PubMed: 3091074]
18. Reddy GK, Enwemeka CS. A simplified method for the analysis of hydroxyproline in biological tissues. Clinical Biochemistry. 1996; 29(3):225–229. [PubMed: 8740508]
19. Boskey A, Camacho NP. FT-IR imaging of native and tissue-engineered bone and cartilage. Biomaterials. 2007; 28(15):2465–2478. [PubMed: 17175021]
20. Camacho NP, West P, Torzilli PA, Mendelsohn R. FTIR microscopic imaging of collagen and proteoglycan in bovine cartilage. Biopolymers. 2001; 62(1):1–8. [PubMed: 11135186]
21. Elliott RJ, Gardner DL. Changes with age in the glycosaminoglycans of human articular-cartilage. Annals of the Rheumatic Diseases. 1979; 38(4):371–377. [PubMed: 496451]
22. Keinan-Adamsky K, Shinar H, Navon G. Multinuclear NMR and MRI studies of the maturation of pig articular cartilage. Magnetic Resonance In Medicine. 2006; 55(3):532–540. [PubMed: 16450338]

23. Torchia DA, Hasson MA, Hascall VC. Investigation of molecular motion of proteoglycans in cartilage by 13C magnetic resonance. Journal of Biological Chemistry. 1977; 252(11):3617–3625. [PubMed: 140875]
24. Ghiassi-Nejad M, Torzilli PA, Peemoeller H, Pintar MM. Proton spin-spin relaxation study of molecular dynamics and proteoglycan hydration in articular cartilage. Biomaterials. 2000; 21(20): 2089–2095. [PubMed: 10966019]
25. Moore GRW, Leung E, MacKay AL, Vavasour IM, Whittall KP, Cover KS, Li DKB, Hashimoto SA, Oger J, Sprinkle TJ, Paty DW. A pathology-MRI study of the short-T2 component in formalin-fixed multiple sclerosis brain. Neurology. 2000; 55(10):1506–1510. [PubMed: 11094105]
26. Laule C, Leung E, Li DKB, Troboulsee AL, Paty DW, MacKay AL, Moore GRW. Myelin water imaging in multiple sclerosis: quantitative correlations with histopathology. Multiple Sclerosis. 2006; 12(6):747–753. [PubMed: 17263002]
27. Rieppo J, Toyras J, Nieminen MT, Kovanen V, Hyttinen MM, Korhonen RK, Jurvelin JS, Helminen HJ. Structure-function relationships in enzymatically modified articular cartilage. Cells Tissues Organs. 2003; 175(3):121–132. [PubMed: 14663155]
28. Lesperance LM, Gray ML, Burstein D. Determination of fixed charge density in cartilage using nuclear magnetic resonance. Journal of Orthopaedic Research. 1992; 10(1):1–13. [PubMed: 1309384]
29. Ling W, Regatte RR, Navon G, Jerschow A. Assessment of glycosaminoglycan concentration in vivo by chemical exchange-dependent saturation transfer (gagCEST). Proceedings of the National Academy of Sciences of the United States of America. 2008; 105(7):2266–2270. [PubMed: 18268341]
30. Shapiro EM, Borthakur A, Gougoutas A, Reddy R. Na-23 MRI accurately measures fixed charge density in articular cartilage. Magnetic Resonance in Medicine. 2002; 47(2):284–291. [PubMed: 11810671]

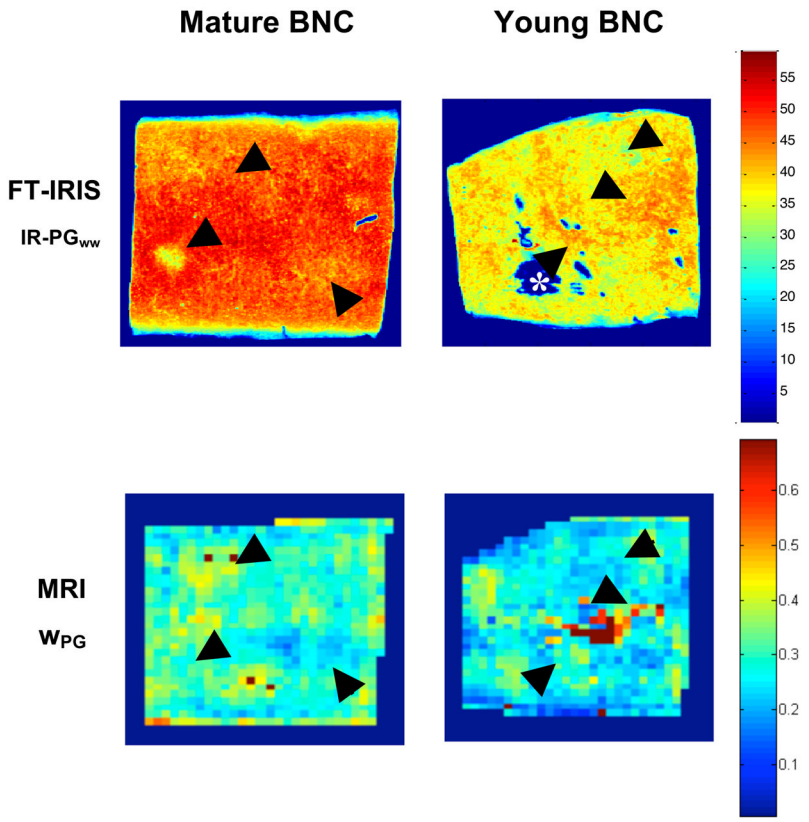

Figure 1.
Representative FT-IRIS normalized PG maps (IR-PG_{ww}) and MRI-derived PG-bound water maps (w_{PG}) from young and mature BNC. Normalization, as described in the text, allows for a more direct comparison between modalities since FT-IRIS measurements are made on histologically prepared tissue sections while MRI measurements are made on intact hydrated samples. Black arrows highlight corresponding regions. An example of the voids caused by histological sectioning is indicated by the white asterisk (*).

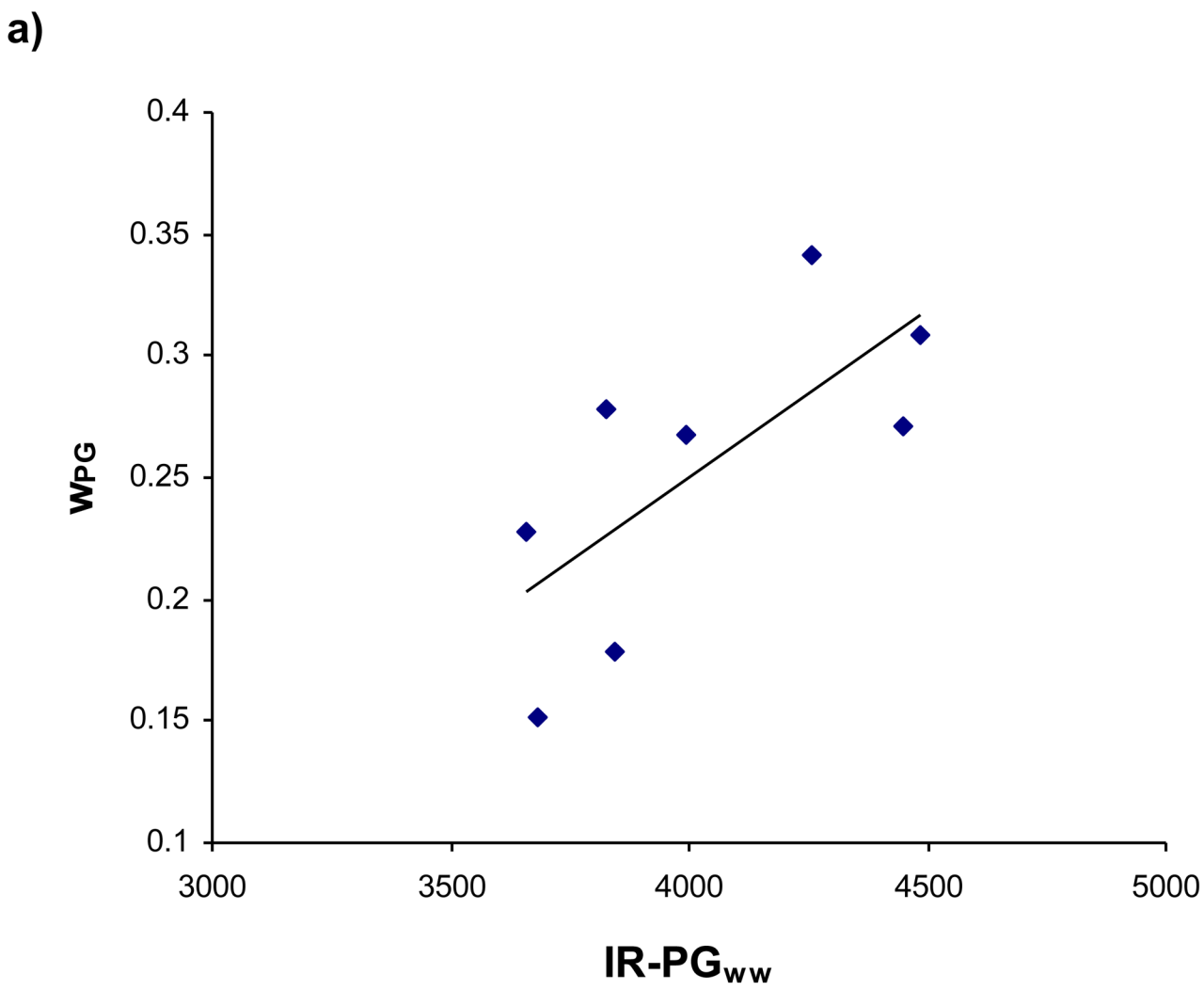

Figure 2.
w_{PG} plotted against FT-IRIS normalized PG content, with regression analysis indicating a significant linear relationship (r = 0.72, P = 0.046).

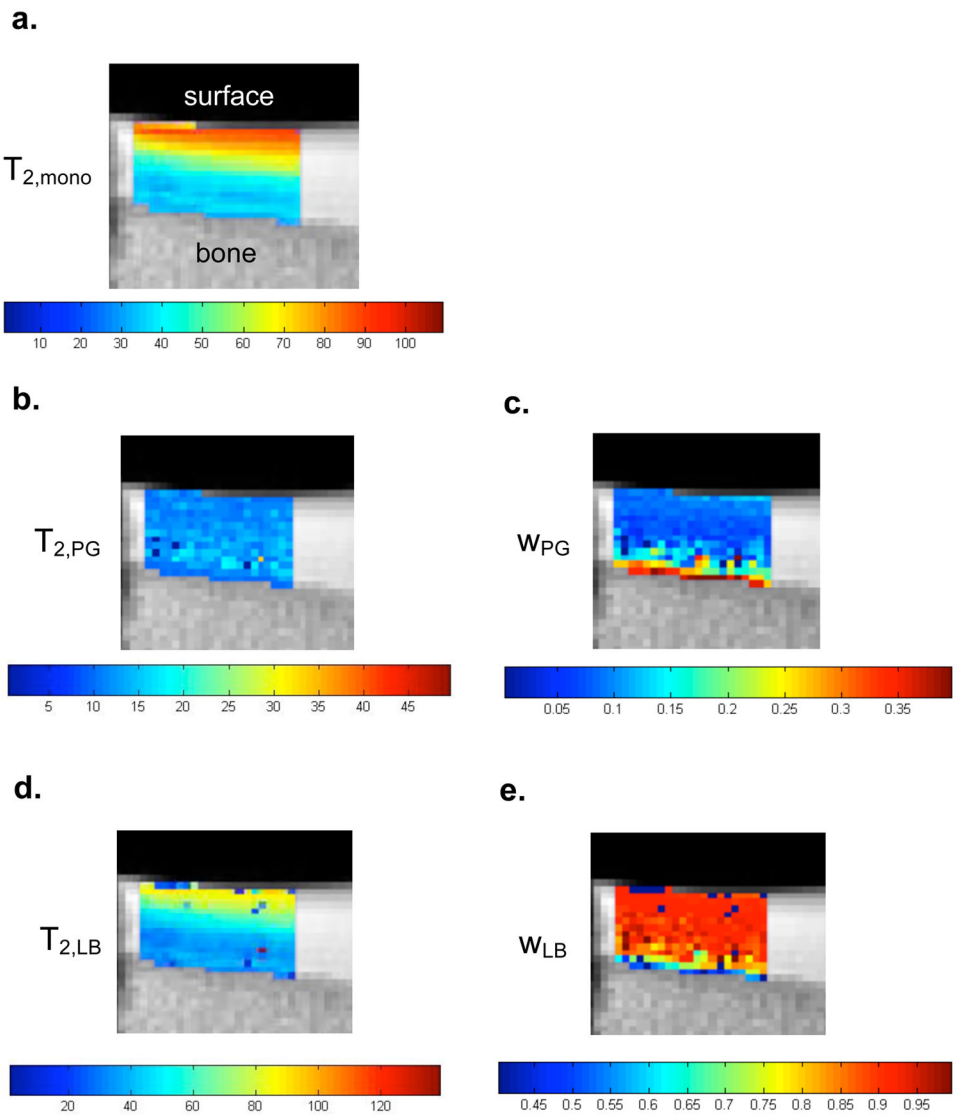

Figure 3.

(a) Monoexponential and (b–e) multiexponential T_2-derived maps from bovine patella cartilage. The monoexponential T_2 map shows a non-specific depth dependence that could be attributable to water content, macromolecular content, and collagen fiber orientation. MR-derived PG (w_{PG}) and water (w_{LB}) maps show depth dependence reflecting PG and water gradients known to exist in articular cartilage.

Table 1

Estimated accuracy and precision of T_2s and associated weights from multiexponential fits.

Group		$T_{2,PG}$	$T_{2,LB}$	w_{PG}	w_{LB}
Young	Accuracy	0.90	0.31	2.11	−0.63
	Precision	1.44	0.29	1.75	0.52
Mature	Accuracy	0.50	0.40	1.84	−0.82
	Precision	1.60	0.32	1.40	0.63

Simulations results for accuracy and precision. Accuracy is defined as average percent error. Precision is reported as the coefficient of variation (CV), defined as the standard deviation over 100 noise realizations divided by the input parameter value × 100. Reliability (not shown), defined as correctly identifying the number of input T_2 components, was 100 percent for both young and mature tissue. Reported values are estimated using the average experimental SNRs of 3,365 and 3,587, for young and mature BNC, respectively. In each case, 100 noise realizations using the average T_2s and associated weights as input values were simulated. Simulation input values for the PG component, C_{PG}, and the loosely-bound water component, C_{LB}, for young and mature tissue were (T_2 ms, % magnetization): young C_{PG} = (27ms, 23%) and C_{LB} = (88ms, 77%); mature C_{PG} = (20ms, 31%) and C_{LB} = (63ms, 69%). Note that in all cases both accuracy and precision were on the order of 2% or less.

Table 2

BNC matrix component quantification using biochemistry.

	Water content (% total weight)	sGAG per d.w. (ug/mg)	sGAG per w.w. (ug/mg)	HP per d.w. (ug/mg)
Young (n = 5)	77.9 ± 0.8	503 ± 45.8	111 ± 9.2	42.4 ± 3.2
Mature (n = 3)	65.7 ± 2.7*	360 ± 27.2*	123 ± 19.4	52.2 ± 9.9

Mature samples showed less water content and sGAG per dry weight than young samples.

* $p < 0.05$ young vs. mature.

Table 3

FT-IRIS- and MR-derived tissue parameters.

	FT-IRIS PG	FT-IRIS Amide I	FT-IRIS IR-PG_{ww}	MRI $T_{2,mono}$ (ms)	MRI w_{PG}
Young (n = 5)	2953 ± 100	2688 ± 37	3801 ± 137	84.5 ± 10.5	0.22 ± .06
Mature (n = 3)	2889 ± 78	3180 ± 79 *	4397 ± 123 *	64.8 ± 6.1 *	0.31 ± .04 *

FT-IRIS results are expressed as areas under absorption bands in arbitrary units. Directly-measured PG content is shown in the first column, while the third column indicates the values for normalized PG content. w_{PG} is the magnetization fraction associated with PG-bound water. Mature samples showed greater collagen as quantified by the amide I band, greater IR-PG_{ww} and w_{PG}, and shorter $T_{2,mono}$.

* $p < 0.05$ young vs. mature.